

Apparent Rates of Fe(II) Oxidation and Associated Hydrogeochemical Interactions in an Extensively Mined Watershed, Pennsylvania, USA

Charles A. CRAVOTTA III

U.S. Geological Survey Pennsylvania Water Science Center, New Cumberland, PA 17070, cravotta@usgs.gov

Abstract Baseflow in the West Branch Schuylkill River, which drains a 61.8 km² watershed in eastern Pennsylvania, consists of coal-mine drainage (CMD) from two large outfalls. During 2005–12, the CMD had elevated Fe(II) concentrations but was net alkaline with near-neutral pH (5.3–7.3). Along a 4,950 m flow path downstream of the outfalls, pH increased by as much as 1 unit and Fe concentrations decreased by 30 to 95 % because of CO₂ degassing and Fe(II) oxidation, respectively. Iron attenuation was greatest during low flows when transport times, pH, and temperature were greatest. Fe(II) oxidation was consistent with the Singer-Stumm abiotic, homogeneous rate model.

Keywords abandoned mines; acid mine drainage; iron oxidation rate

Introduction

The Schuylkill River in eastern Pennsylvania, USA, has its headwaters in uplands of the Southern Anthracite Coalfield and its mouth 208 km downstream, on the Delaware River at Philadelphia (Fig. 1). Because of extensive infiltration to abandoned underground mines, streams in the headwaters frequently lose water and may stop flowing, while perennial

streamflow is sustained downstream by coal mine drainage (CMD). The Pine Knot Tunnel (PKN), a very large CMD source (0.25 – 1.59 m³/s), and the Oak Hill Boreholes (OAK), a smaller CMD source (0.096 – 0.48 m³/s) near the midpoint length of the West Branch Schuylkill River (Fig. 1), account for one-third of the contaminant loading by several dozen CMD sources to the upper Schuylkill River

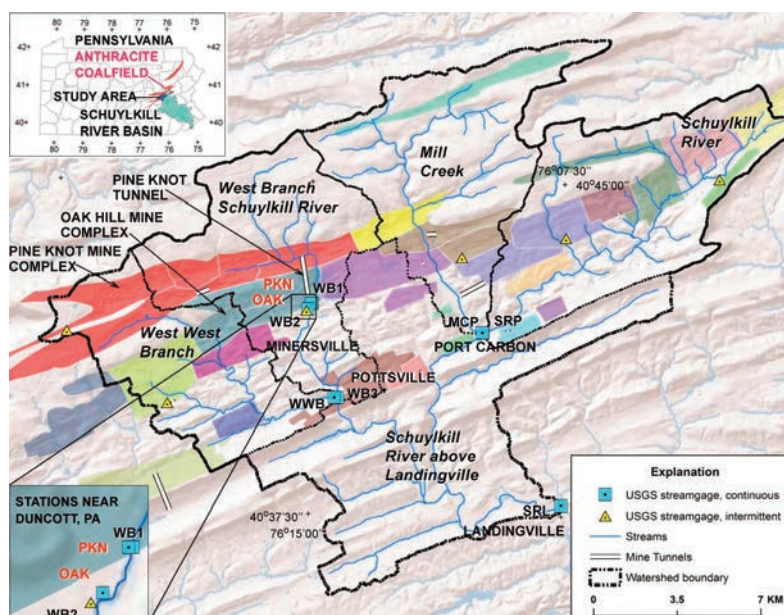


Fig. 1 Drainage basins, underground mines (colored polygons), and hydrological monitoring sites in the upper Schuylkill River basin, Southern Anthracite Coalfield, Pennsylvania. Descriptions of the mines and monitoring sites are given by Cravotta et al. (2013). Adjacent mines with same color are hydrologically connected. For example, the Pine Knot mine complex comprises five adjoining mines.

(Cravotta *et al.* 2013). The discharge of PKN responds rapidly to recharge but has a prolonged recession compared to the West Branch Schuylkill River and other nearby streams, consistent with a conceptual model of rapid infiltration of surface water and slow release of groundwater from the underground mine complex. During seasonal low-flow conditions when the streams in the headwaters lose all flow to the underground mines, these CMD sources constitute the entire streamflow from the 61.8 km² watershed of the West Branch Schuylkill River. In contrast, during high-flow conditions, streamflow from the headwaters area frequently exceeds the combined flows of the CMD sources (Cravotta *et al.* 2013). This paper evaluates hydrogeochemical interactions that account for the temporal and spatial variations in the concentrations and transport of iron and associated solutes from CMD sources at downstream sites in this extensively mined watershed.

Methods

Data on flow rate, pH, alkalinity, acidity, and concentrations of total and dissolved elements (0.45- μ m pore-size, 45 mm diameter nitrocellulose membrane filter) were collected over a range of hydrologic conditions during 2005–12 at the PKN and OAK outfalls and associated upstream and downstream sites on the West Branch Schuylkill River (Fig. 1). When samples were collected, temperature, pH, specific conductance (SC), dissolved oxygen (DO), and redox potential (Eh) were measured with a submersible sonde that was calibrated daily. Values for Eh were corrected to 25 °C relative to the standard hydrogen electrode and used to compute the activities of Fe(II) and Fe(III) species from dissolved iron (Nordstrom 1977, 2004). The geochemical program PHREEQC (Parkhurst and Appelo 1999) with WATEQ4F database (Ball and Nordstrom 1991) was used to evaluate the equilibrium partial pressure of carbon dioxide (Pco₂), the saturation index values for various minerals, and mass-balance reactions to explain the composition of (1)

downstream water from mixtures of upstream waters and (2) high-flow water from base flow plus runoff. Apparent first-order Fe(II) oxidation rates within the West Branch were estimated based on the decrease in dissolved iron concentration along a 4,950 m flow path from station WB2 downstream of the two CMD outfalls to station WB3 near the mouth of the West Branch watershed (Fig. 1). Transport times, calculated as reach distance divided by velocity at the downstream gaging station (WB3), were estimated on the basis of empirical relations among the average velocity measured by current meter across the channel, associated discharge rate, and stream stage at the time of sampling. The stream channel between WB2 and WB3 has relatively uniform shape and slope. Apparent first-order Fe(II) oxidation rates were computed on the basis of the estimated transport time and also considering data on pH, DO, and temperature.

Results and Discussion

CMD a PKN and OAK was net alkaline (acidity < 0) with near-neutral pH (5.3 to 7.3), elevated concentrations of sulfate, iron, and manganese, and relatively low concentrations of aluminum (Fig. 2). Streamwater quality of the West Branch above PKN (WB1) varied from net acidic to alkaline (pH 3.9 to 6.8; acidity 210 to -9.1 mg/L); however, streamwater at sites downstream of the CMD sources (WB2 and WB3) consistently was net alkaline with near-neutral pH (Fig. 2). The pH and concentrations of dissolved iron in CMD at PKN decreased with increased flow rate (Spearman's $r_s = -0.69$ and -0.63 , respectively; $P < 0.001$; Fig. 2). Likewise, dissolved iron concentration was inversely correlated with CMD flow rate at the Oak Hill Boreholes ($r_s = -0.64$; $P < 0.001$). At sites on the West Branch upstream (WB1) and downstream (WB2 and WB3) of the CMD outfalls, pH, SC, sulfate, and other major ion concentrations decreased with increased flow rate; however, dissolved iron concentrations did not vary with flow rate at sites WB1 and WB3 (Fig. 2).

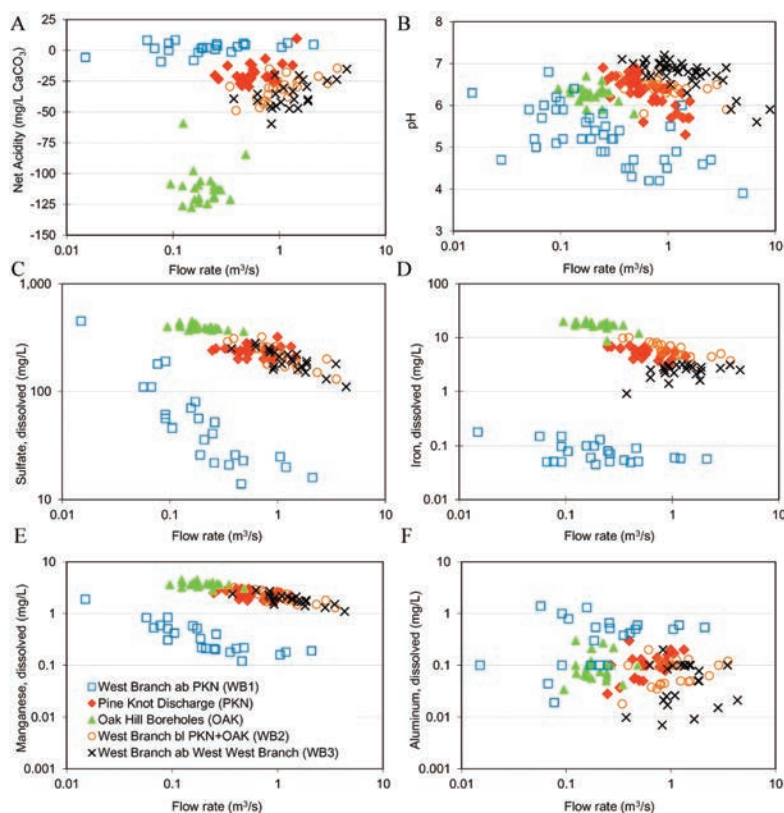


Fig. 2 Discharge rate and water quality of CMD from the Pine Knot Tunnel (PKN) and Oak Hill Boreholes (OAK), and associated stream water from West Branch above PKN (WB1), and West Branch below PKN and OAK at intermediate (WB2) and downstream (WB3) sites, July 2005–July 2012.

During high-flow conditions, the CMD and stream waters exhibited increased acidity with decreased pH and smaller changes in iron concentrations and pH along downstream flow paths (Figs. 2 and 3). These water-quality characteristics at the downstream sampling point WB3 were modeled by starting with the water quality at WB2 below the CMD outfalls and considering geochemical reactions, with or without dilution by runoff. For the low-flow end members (sampled 2008/09/24) when flows at WB2 and WB3 were comparable, geochemical mass-balance reactions, alone were indicated, including ingassing of O_2 , degassing of CO_2 , dissolution of halite, and precipitation of ferrihydrite and $Al(OH)_3$. For the high-flow end members (sampled 2010/03/16), the flow at WB3 ($4.33 \text{ m}^3/\text{s}$) was larger than that at WB2 ($3.51 \text{ m}^3/\text{s}$). Thus, flow-weighted fractions of 0.81 WB2 and 0.19 "runoff" having low pH and low ionic strength were mixed, and the indicated mass-balance reactions included degassing of CO_2 , dissolution of halite, calcite,

and chlorite, plus precipitation of $Al(OH)_3$ and ferrihydrite. The degassing of CO_2 and the precipitation of $Al(OH)_3$ and ferrihydrite in low-flow and high-flow models is consistent with the attenuation of the metals from CMD in conjunction with pH increases over the range of flow conditions (Fig. 2). The indicated dissolution of halite and calcite is consistent with the addition of road-deicing salts and limestone aggregate that are used in the urbanized area downstream of WB2 (Minersville, Pottsville; Fig. 1).

At WB2, dissolved and total iron concentrations ranged from 3.2 to 10 mg/L and 3.9 to 11 mg/L, respectively, pH ranged from 5.9 to 6.8, and P_{CO_2} ranged from $10^{-2.2}$ to $10^{-1.1}$ atm. Along the 4,950-m flow path from WB2 to WB3, dissolved iron concentrations decreased by 30 to 95 % whereas total iron decreased by 3 to 70 %, pH increased by as much as 1 unit, P_{CO_2} decreased by 40 to 80 %, and sulfate and manganese concentrations were largely unchanged (Fig. 3). Sulfate and manganese

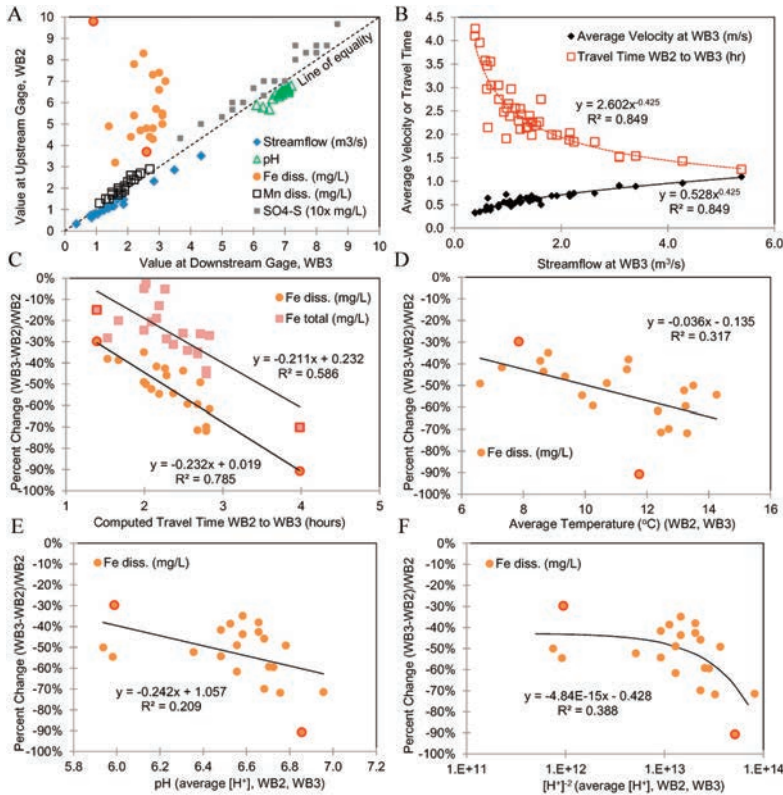


Fig. 3 Attenuation of dissolved iron and associated constituents along 4,950 m flow path from WB2 to WB3 on West Branch Schuylkill River, July 2005-July 2012. A, Comparison of streamflow and water quality at WB2 and WB3; B, streamflow, average flow velocity, and computed time to travel from WB2 to WB3; C-E, change in dissolved iron concentration as a function of travel time, temperature, pH, and $[H^+]^{-2}$. Low-flow and high-flow end members considered in geochemical models highlighted by red outline.

(Mn(II)) were transported conservatively because these solutes were undersaturated with respect to secondary minerals. The attenuation of dissolved iron resulted from the gradual oxidation of ferrous iron (Fe(II)) to ferric iron (Fe(III)) and the rapid precipitation of hydrous Fe(III) oxides such as ferrihydrite, which was saturated or supersaturated (Cravotta *et al.* 2013). Because of the low solubility of Fe(III) at near-neutral pH, nearly all the dissolved iron was Fe(II). The pH increased downstream because of degassing of CO₂ as observed for other iron-bearing, net-alkaline waters exposed to the atmosphere (Cravotta 2007; Kirby *et al.* 2009; Geroni *et al.* 2012).

Attenuation of dissolved iron downstream of CMD sources was greatest during low-flow conditions when transport times, water temperatures, and pH values were greatest (Fig. 3). These trends indicate a kinetically limited process and are consistent with the abiotic homogeneous oxidation rate model of Singer and Stumm (1970) as presented by

Stumm and Morgan (1996, 683–685):

$$-d[Fe(II)]/dt = k_H \cdot [O_2] \cdot [H^+]^{-2} \cdot [Fe(II)] \quad (1)$$

where at pH > 5 and 20 °C, $k_H = 3 \times 10^{-12}$ mol/L/min (1.8×10^{-10} mol/L/h). The second-order dependence on $[H^+]$ indicates a change in pH of 1 unit results in a 100-fold change in the oxidation rate. At a given pH, the rate increases by a factor of 10 for a 15 °C increase. By using the activation energy of 23 kcal/mol reported by Stumm and Morgan (1996, p. 684) with the Arrhenius equation (Langmuir 1997, p. 62), the rate can be adjusted to different temperatures.

Fig. 4A illustrates the apparent first-order rate of change in dissolved iron concentration from WB2 to WB3, without temperature correction, as a function of $[O_2][H^+]^{-2}$ per Eq. 1. The simple first-order rate (Y-axis) ranges from 0.22 to 0.60/h with a median of 0.34/h at average temperature of 10.83 °C. The slope in Fig. 4A, 9.14×10^{-12} mol/L/h at 10.83 °C, is one-fifth

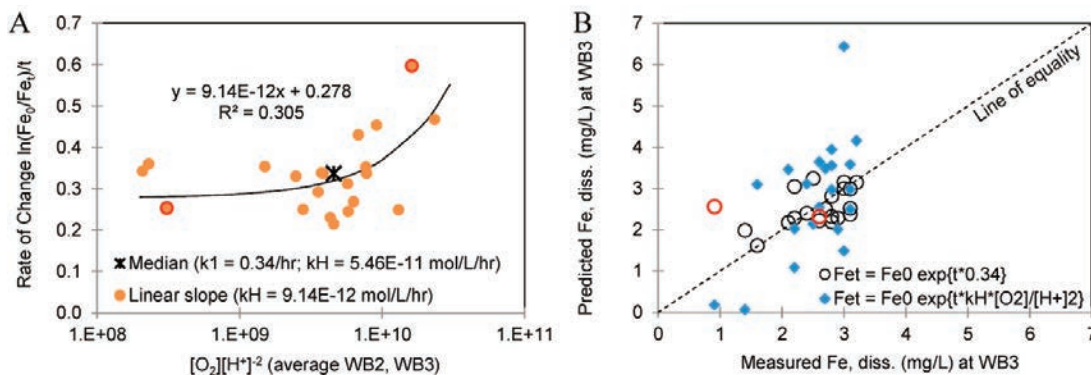


Fig. 4 A, Apparent first-order rate of Fe(II) oxidation without temperature correction is indicated by median value of 0.34/h, or as a function of $[O_2][H^+]^{-2}$ based on Eq. 1, in which case k_H^* is indicated as the ratio of the rate value to $[O_2][H^+]^{-2}$ (5.46×10^{-11} mol/L/h at 10.83 °C) or the slope; B, measured and predicted dissolved iron concentration at WB3 on the basis of dissolved iron concentration at WB2, travel time, average temperature, average dissolved O_2 , and average $[H^+]^{-2}$ for WB2 to WB3. Circles indicate predicted values considering median first-order rate of 0.34/h and blue diamonds indicate predicted values considering Eq. 1 with temperature-corrected median apparent rate constant, $k_H^* = 1.95 \times 10^{-10}$ mol/L/h (3.26×10^{-12} mol/L/min) at 20 °C.

of the reference value of k_H for Eq. 1 given by Stumm and Morgan after temperature adjustment to 20 °C. The median ratio of the first-order rate to $[O_2][H^+]^{-2}$ (5.46×10^{-11} mol/L/h at 10.83 °C) adjusts to $k_H^* = 3.26 \times 10^{-12}$ mol/L/min at 20 °C, which is equivalent to the reference value of k_H for Eq. 1. The median ratio using the flow-weighted concentration (mass change) is similar, 2.29×10^{-12} mol/L/min at 20 °C.

Fig. 4B shows the predicted concentration of dissolved iron at WB3 based on the concentration at WB2 and estimated travel time to WB3 by using (1) the median first order decay rate of 0.34/h, without temperature or pH adjustment, and (2) the homogeneous oxidation rate model of Eq. 1 with the median apparent rate constant of $k_H^* = 3.26 \times 10^{-12}$ mol/L/min at 20 °C adjusted for sample temperature. Despite consideration of variable temperature, pH, and dissolved O_2 , the estimate with Eq. 1 does not yield significant improvement over the simple first-order estimate. A constant first-order rate may apply because of the relatively narrow range of temperature (10 ± 4 °C) and pH (6.6 ± 0.2) for most samples and their

correlation with flow rate. Kirby *et al.* (1999) demonstrated that abiotic Fe(II) oxidation predominates over microbial catalysis at pH values greater than 5 and that pH increases above 6.4 had little to no effect on Fe(II) oxidation rate.

Conclusions

Observed water-quality and discharge relations for CMD and downstream sites on the West Branch Schuylkill River indicate decreased attenuation of iron with decreased transport time, decreased temperature, and decreased pH. These trends are consistent with kinetic control of Fe(II) oxidation, consistent with the Singer-Stumm abiotic, homogeneous rate model. The inverse relations between flow rate and pH can result from mixing of near-neutral CMD with low-pH runoff or recharge derived from acidic rainfall. Given kinetically controlled, pH-dependent iron attenuation, potential decreases in pH (< 6.4) during high-flow events should be considered with strategies to decrease iron loads. Specifically, if aerobic ponds or wetlands are used for treatment of marginally net alkaline CMD, a supplement-

tal source of alkalinity may be needed to maintain or increase pH during high flow conditions as well as additional storage capacity may be needed to increase retention time.

References

- Ball JW, Nordstrom DK (1991) User's manual for WATEQ4F with revised data base. U.S. Geol. Surv. Open-File Report 91-183, 189 p
- Cravotta CA III (2007) Passive aerobic treatment of net-alkaline, iron laden drainage from a flooded underground anthracite mine, Pennsylvania, USA. *Mine Water Environ.* 26, 128–149
- Cravotta CA III, Goode DJ, Bartles MD, Risser DW, Galeone, DG (2013) Surface-water and groundwater interactions in an extensively mine watershed, upper Schuylkill River, Pennsylvania, USA. *Hydrol. Proc.* doi: 10.1002/hyp.9885
- Geroni JN, Cravotta CA III, Sapsford DJ (2012) Evolution of the chemistry of Fe bearing waters during CO₂ degassing. *Appl. Geochem.* 27: 2335–2347
- Kirby CS, Dennis A, Kahler A (2009) Aeration to degas CO₂, increase pH, and increase iron oxidation rates for efficient treatment of net alkaline mine drainage. *Appl. Geochem.* 24, 1175–1184
- Kirby CS, Thomas HM, Southam G, Donald R (1999) Relative contributions of abiotic and biological factors in Fe(II) oxidation in mine drainage. *Appl. Geochem.* 14, 511–530
- Langmuir D (1997) *Aqueous environmental geochemistry*. Prentice Hall, New Jersey, USA, 600 p
- Nordstrom DK (1977) Thermochemical redox equilibria of Zobell's solution. *Geochim. Cosmochim. Acta* 41, 1835–1841
- Nordstrom DK (2004) Modeling low-temperature geochemical processes. In Drever JL (ed.) *Surface and Ground Water, Weathering, and Soils*. Elsevier, *Treatise on Geochemistry* 5, 37–72.
- Parkhurst DL, Appelo CAJ (1999) User's guide to PHREEQC (Version 2)—A computer program for speciation, batch-reaction, one-dimensional transport, and inverse geochemical calculations. U.S. Geol. Surv. Water-Resour. Inv. Re99-4259, 310 p
- Singer PC, Stumm W (1970) Acidic mine drainage: the rate-determining step. *Science* 167, 121–123
- Stumm W, Morgan JJ (1996) *Aquatic chemistry—chemical equilibria and rates in natural waters* (3rd). New York, Wiley-Interscience 1022 p